

DOI: 10.13208/j.electrochem.170143

Artical ID:1006-3471(2017)04-0391-09

Cite this: *J. Electrochem.* **2017**, 23(4): 391-399

Http://electrochem.xmu.edu.cn

Electrostatic Interactions of Water in External Electric Field: Molecular Dynamics Simulations

Zhu Qiang, Kan Zi-gui, Ma Jing*

(Key Laboratory of Mesoscopic Chemistry of MOE School of Chemistry & Chemical Engineering,
Nanjing University, Nanjing, 210093, China)

Abstract: A series of molecular dynamics simulations with or without external electric field have been carried out for bulk water with periodic boundary condition. The difference in radial distribution function of interatomic O...O distance is subtle, with and without external electric field, except for the orientation of dipole moments of water molecules. Without the applied external electric field, distribution of the orientation angle of dipole moments is rather broad. The induced local electric field is analyzed as a function of altitude in direction of electric field. The variation of the local induced electric field is increased with the increase of the external electric field. The local induced electrostatic energy is mainly originated from the increase in the ordering of dipole orientation under the external electric field. Dielectric constant is evaluated according to the fluctuation of total dipole moment in the whole system. The change of relative dielectric constant under the different external electric fields can be described in an exponential decay equation as the increase in the strength of electric field. This simple rule can be applied to understand the electrostatic interaction and local induced electric field under various electrochemical environments.

Key words: radial distribution function; dielectric constant; uniform electric field model; induced electric field; dipole moment

CLC Number: O646

Document Code: A

The simplicity of continuum electrostatic model makes it popular in accounting for the long-ranged electrostatics interactions in biological and materials systems. As a consequence, the choice of the dielectric constant is the key to mimic the environment of the studied systems^[1]. Dielectric constant is usually measured under some mild conditions^[2], however, it is difficult to perform the measurement under some extreme conditions such as high pressure, high temperature, and the interfacial electrochemical reactions with complicated composition. Using the molecular dynamics (MD) simulations to investigate the dielectric constant is becoming increasingly appealing. Wasserman et al. have investigated the dielectric constant under high pressure and high temperature conditions using the extended simple point charge water model (SPC/E)^[3]. They claimed that the SPC/E water

model could reproduce the experimental data over a wide range of temperature and pressure^[3]. The employment of either the Kubic technique or the Ewald methods resulted in no difference in the estimation of the dielectric constant, and no evidence was shown to support that the applied electric field could speed up the convergence rate^[3].

A lot of water models, with polarizable or non-polarizable force field, such as SPC/E^[4], TIP3P^[5], TIP4P^[5], and MCDHO^[6], have been implemented to reproduce the physical properties of water. It is still a big challenge for theoretical chemists to reproduce all the experimental data, such as the liquid density, temperature, pressure, heat of vaporization, the dielectric constant and so on^[7]. A systematic study suggested that, to get a good estimation of the dielectric constant, trajectories should be longer than 6 ns, in addition, the

model size and the methods for controlling the temperature could affect the dielectric constant strongly^[8]. Sprik also compared the performance of different water models (TIP4P, SRWK and their corresponding polarizable models)^[9]. It was claimed that, dielectric constant was dependent on the magnitude of the dipole moment strongly, and to get the correct dielectric constant, the average dipole moment for a water molecule should fall in a range of 2.5 ~ 2.6 Debye^[9].

However, the dependence of dielectric constant on the external electric field was rarely studied until now. By using the MD simulation, Yeh presented that^[10], regardless of the choice of the boundary conditions, the dielectric constant varied a little, and a threshold value, 5 ~ 10 V·nm⁻¹, of the applied electric field was proposed for the water to undergo reconstructing transitions. The ordered and ice-like phase was observed at external field, 30 V·nm⁻¹, and red shift of the frequency spectrum was found when the external electric field was increased^[11]. The present work attempts to give an insight into how the dielectric constant is reflected by the conformational changes of water under different electric fields, and to analyze the relationship between the external field and the induced local electric field of the system we studied.

This work was organized in the following sections. The theoretical model and the technical details of MD simulations were summarized in the section of the computational methods; Subsequently, in the section of results and discussion, results for the O...O radial distribution function were shown, as well as the distribution of orientation angle of water molecule. Furthermore, the trend in ratio of dielectric constant under different external fields was drawn as a function of the strength of electric field. Finally, the induced local electric field under different external field, as well as the relationship between the total electrostatic energy and the external electric field were presented. Our results will give an exponential decay trend of the relative dielectric constant with the increasing strength of electric field and the detailed microscopic picture, which are applicable to study

the electrostatic polarization and distribution of local induced electric field in various interesting electrochemical environments.

1 Computational Methods

Independent MD simulations were carried out using software NAMD^[12], GROMACS^[13] and AMBER^[14]. TIP3P was selected for the water model. In the scheme of NAMD and AMBER, the dimension of initial box was 25.0 Å × 25.0 Å × 25.0 Å. It was composed of 464 water molecules in the cubic cell, the total number of atoms in the system was 1392. In the MD simulation with GROMACS, the initial setting was slightly different: 466 water molecules were added in the cubic box of 24.0 Å × 24.0 Å × 24.0 Å. All MD simulations were performed in the cubic box with the periodic boundary condition.

We performed MD simulations in the NPT ensemble until the density of the box approached the value that obtained from the experiments (1.0 kg·m⁻³), the final dimension of box was 23.8 Å × 23.8 Å × 23.8 Å, and the corresponding density was 1.03 kg·m⁻³. The system was equilibrated at constant temperature ($T = 310.0$ K) and pressure (1 atm), MD trajectory was saved in an interval of 10 femtoseconds. The Langevin dynamics parameters and Nose-Hoover Langevin piston were used to maintain the temperature and pressure. To incorporate the polarizable effect, the bond is set to be flexible^[15].

In all simulations, no matter in which ensembles, the cutoff distance of van der Waals interaction and electrostatic interactions were both set to 12 Å. The switch distance was 10 Å, which ensured the potential to be smoothly reduced to 0 at the assigned distance. In addition, particle mesh Ewald (PME) was applied for the periodic boundary conditions.

The system performed at NPT ensemble was equilibrated for 100 ps. Subsequently, the rest simulations in NVT ensemble were run for 30 ns (without external electric field), and 10 ns (with different external electric fields), respectively, long enough for the convergence of the dielectric constant^[6,15]. The external electric field applied in our simulations was a homogeneous one using a constant electric potential.

2 Results and Discussion

2.1 Changes of Conformation and Dipole Moments under Electric Field

To investigate how the structure changed when the external electric field, E_{ext} , was applied, the radial distribution function, g_{oo} , was introduced to show the probability of finding an oxygen atom at an inter-atomic $\text{O}\cdots\text{O}$ distance, from the other oxygen atom, as defined bellow:

$$g_{\text{oo}}(r) = \frac{dN}{\rho \times 4\pi r_{\text{oo}}^2 dr} \quad (1)$$

where dN represents the particle numbers between r_{oo} and $r_{\text{oo}} + dr$, ρ is the system density. The value of $g_{\text{oo}}(r)$ can be interpreted as the ratio of local density to bulk density. The local density is different from the bulk density when the distance r_{oo} is close to the reference molecule, but they are the same when the distance is large enough.

The radial distribution functions of two oxygen atoms under different external electric fields are shown in Fig. 1. No matter how strong was the external electric field applied, the difference between radial distribution function of two oxygen atoms was rather subtle. The first peak under different external electric fields all occurred at 3 Å, then they passed through a minimum value around $r = 4.5$ Å. The second peak was found to locate at the 5.5 Å. The first peak and corresponding matched well with the experimental results derived from the neutron diffraction data^[16-18].

Despite of the negligible difference in radial distribution function of two oxygen atoms caused by the electric field, the orientation of each water molecule was observed to differ a lot from zero filed to $-2.175 \text{ V} \cdot \text{nm}^{-1}$ ($-5 \times 0.435 \text{ V} \cdot \text{nm}^{-1}$). In consideration of the varied degrees of the orientation of water molecule and the dipole moments, as a consequence, both the magnitude and orientation of molecular dipole moment were analyzed (Fig. 2A). As shown in Fig. 2B, the orientation of dipole moment was defined as angle, θ , which is the angle formed between the dipole moment, $\vec{\mu}$, and the z axis. The distributions of orientation angle, θ , presented in Fig. 2 were the averaged

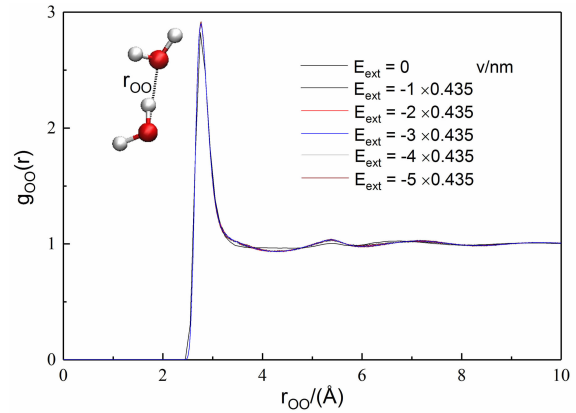


Fig. 1 Radial distribution function, $g_{\text{oo}}(r)$, under different external electric fields.

values over the last 1 ns of each MD simulation under different electric fields.

As shown in Fig. 2A, in the absence of electric field, water oriented freely, so the orientation angle, θ , ranged from 30 to 150 degrees with comparable probabilities. Once the external electric field was added on the opposite direction of z direction in simulation box (Fig. 2B), the water molecule directed in the same orientation parallel to the electric field (Fig. 2C). As the strength of the E-field increased, more ordered orientation was observed for the water molecule. The orientation angle under such condition is between 150 and 180 degrees. This can be reflected from Fig. 3A, which is the selected snapshot at 10 ns with $E_{\text{ext}} = -4 \times 0.435 \text{ V} \cdot \text{nm}^{-1}$. In contrast, the water molecules packed disorderly without the applied external electric field (Fig. 3B).

2.2 Changes of the Dielectric Constant under External Electric Fields

One can use the variance of the total dipole moments \vec{M} of system to estimate the dielectric constant, ε , as expressed as follows^[19]:

$$\varepsilon - 1 = \frac{4\pi}{3k_B T V} (\langle \vec{M}^2 \rangle - \langle \vec{M} \rangle^2) \quad (2)$$

Where k_B is the Boltzmann constant, T is the temperature and V denotes the volume of the simulation box. \vec{M} is the vector sum of each dipole moment $\vec{\mu}_i$ of N individual water molecules, denoted as bellow:

$$\vec{M} = \left(\sum_{i=1}^N \vec{\mu}_i \right)^2 \quad (3)$$

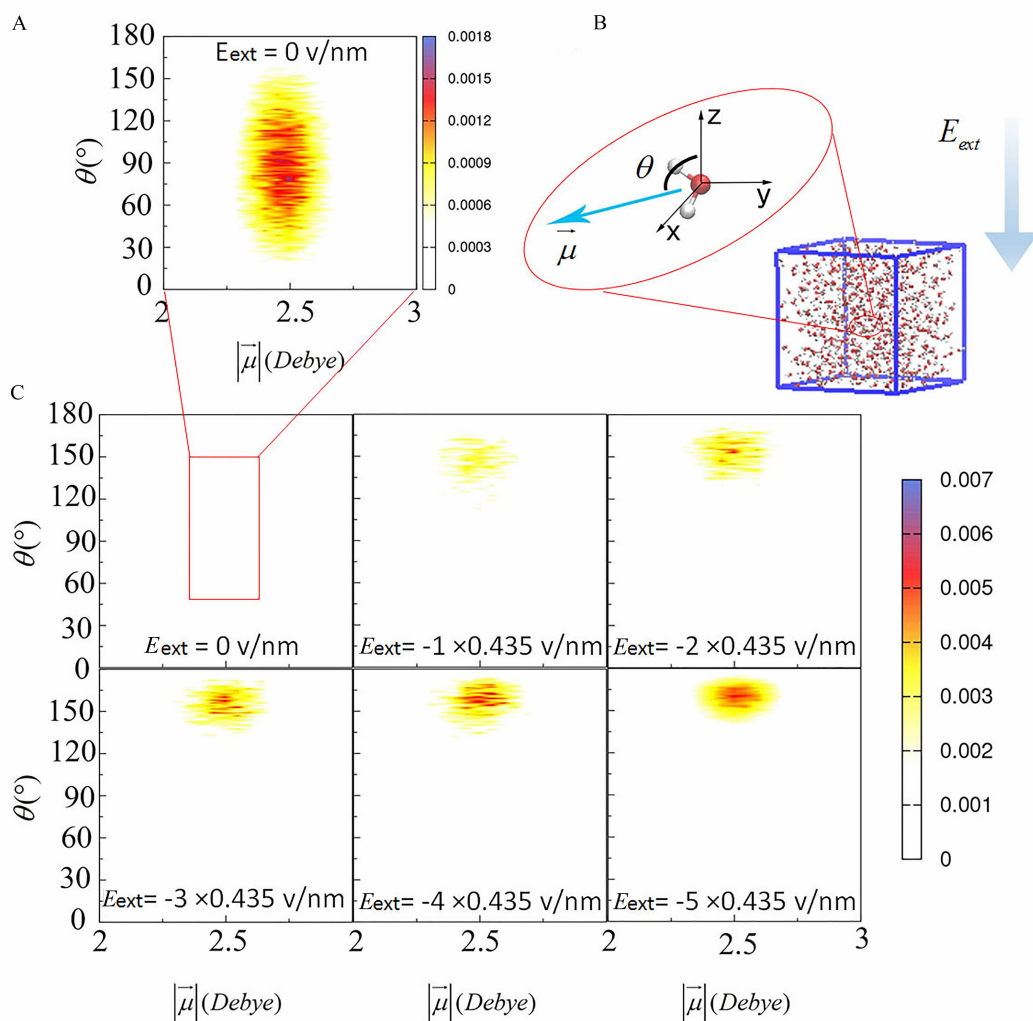


Fig. 2 Magnitude of dipole moment and orientation angle, θ , of individual water molecules in MD trajectories. A. Zoomed figure without external electric field; B. Illustration of the orientation angle θ ; C. Distributions of magnitude of dipole moment and orientation angles under different external electric fields. X-axis represents magnitude of the dipole moment of individual water molecule in unit of Debye. Y-axis represents the orientation angle, θ , in unit of degree.

The parameter G_k was related to the fluctuation of the total dipole moments of the simulation cell, which was estimated from Equation 4^[20].

$$G_k = \frac{\langle \vec{M}^2 \rangle - \langle \vec{M} \rangle^2}{N\mu^2} \quad (4)$$

The convergence rate of G_k was a criterion to reflect how fast the convergence was reached. The variation of G_k under different electric fields is shown in Fig. 4. With the application of external electric field, 10 ns MD was performed for each electric field after 30 ns run without external E-field. In Fig. 4, the last 6 ns trajectory of each simulation was taken to calculate

G_k . The results indicated that the external electric field could accelerate the convergence of the simulation. It was different from the conclusion made in previous work^[3], where a NVE ensemble was taken, and the magnitude of the external electric field was $0.0985 \text{ V} \cdot \text{nm}^{-1}$, much smaller than that $2.175 \text{ V} \cdot \text{nm}^{-1}$ in our work.

Independent MD simulations on dielectric constant, ϵ , have been carried out by using GROMACS, AMBER, and NAMD. Without external electric field ($E_{\text{ext}} = 0 \text{ V} \cdot \text{nm}^{-1}$), the simulated value of static dielectric constant, $\epsilon(0)$, using GROMACS software is 93.64, which coincided well with the literature value $(92 \pm 5)^{[21]}$.

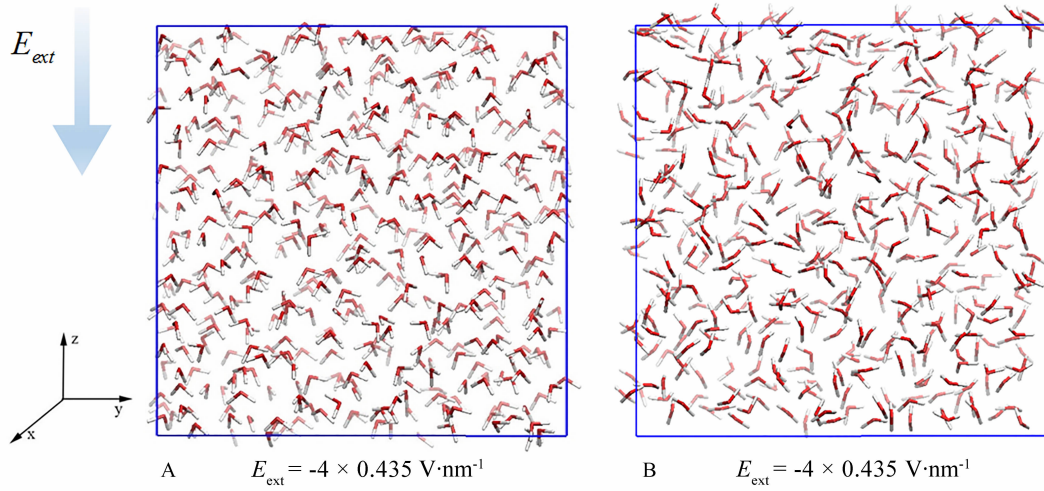


Fig. 3 The selected snapshots of two simulation cases. A. 10 ns under an external electric field with $E_{\text{ext}} = -4 \times 0.435 \text{ V} \cdot \text{nm}^{-1}$; B. 15 ns without external electric field.

However, the estimated dielectric constant is dependent not only on the choice of the force fields of water models, but also on the setting of different softwares, as already being pointed out in many previous works^[9,21-23]. In this work, we laid an emphasis on the change of the relative dielectric constant under different electric fields, $\varepsilon(E_{\text{ext}})$, thus, the ratio of $\varepsilon(E_{\text{ext}})/\varepsilon(0)$ is listed in Table 1 for comparison.

It has been addressed that, when the external electric field is small (i.e. $\mu E_{\text{ext}} \ll 3k_{\text{B}}T$), the dielectric constant is linear in the external electric field^[24]. In this work, the value of is about $8.77 \times 10^{10} \text{ K}$ when $E_{\text{ext}} = -0.435 \text{ V} \cdot \text{nm}^{-1}$, much larger than the room tem

perature. Under such a strong external electric field, the dielectric constant exponentially decays with the increased external electric field, E_{ext} . As shown in Fig. 5, the value of decreases along with the increasing strength of external E-field. An exponential decay function was fitted from the calculation results, as presented by Equation 5.

$$\frac{\varepsilon(E_{\text{ext}})}{\varepsilon(0)} = 0.48e^{-1.85E_{\text{ext}}} + 0.46e^{-9.25E_{\text{ext}}} + 0.06 \quad (5)$$

Where $\varepsilon(E_{\text{ext}})$ represents the dielectric constant under certain external electric field, and $\varepsilon(0)$ denotes the one without external electric field.

As depicted in the Figure 5 and Table 1, when the external field raised up to $-0.435 \text{ V} \cdot \text{nm}^{-1}$, the ratio of decreased steeply to 0.28. This trend is similar to what was obtained by Yeh's^[10] simulations of bulk water, using 3-D Ewald summation, under the external electric field of 0.525, 1.22, and $5 \text{ V} \cdot \text{nm}^{-1}$ (hollow circle in Figure 5), respectively. The difference in the decay speed of field-dependent dielectric constant with the increasing strength of electric field between ours and Yeh's results is ascribed to the choice of the models and parameters of force fields. In addition, Yeh used the SHAKE algorithm^[20] to preserve the rigidity of the water molecules, while we used the flexible water in the present work. And the times scale of ours (10 ns) is 100 times of theirs (100 ps).

2.3 The Local Induced Electric Field

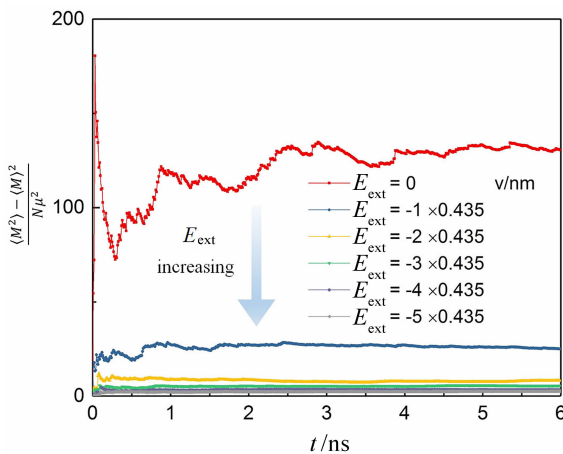


Fig. 4 Converge test of G_k . Each MD simulation under electric field was performed for 10 ns (after the 30 ns MD simulation without E-field)

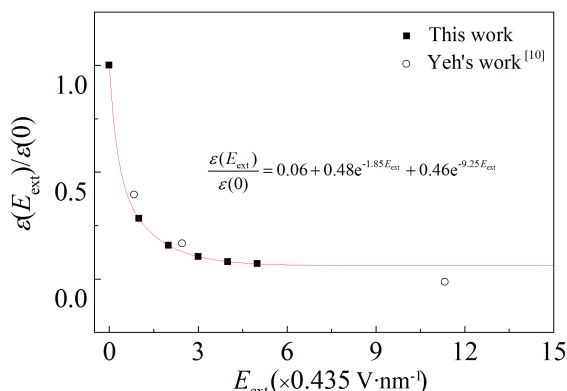


Fig. 5 Trend of relative dielectric constant to the zero-field case under different external electric fields, as shown by the fitting curve derived from the calculated points.

Having possessed the relative dielectric constants under different electric fields, the induced local electric field was predicted as a function of relative position along the direction of the electric field. Assumption was made that the x and y components of the induced field should be zero in two parallel plates, and the local E -field was only dependent on the position where the attitude in z -direction.

The local electric field was achieved by a Tool Command Language (TCL) script written by ourselves embedded in the VMD^[25], which was implemented in the following procedure: (a). Slicing the system into N_{slab} slabs evenly as shown in Fig. 6A; (b). For each slab, total charge at each side was summed, and denoted as the $Q(Z_{\text{lower}})$ and $Q(Z_{\text{upper}})$, respectively; (c). Using Equation 6 to calculate the local electric field. The induced electric field, $E_{\text{ind}}(z)$, in z -direction could be estimated by the following expression^[26]:

$$E_{\text{ind}}(z) = \frac{\langle Q(Z_{\text{lower}}) \rangle - \langle Q(Z_{\text{upper}}) \rangle}{2 \times \varepsilon(E_{\text{ext}}) \times A} \quad (6)$$

where $\langle Q(Z_{\text{lower}}) \rangle$ represents the total charges below Z_{lower} averaged over n frames, $\langle Q(Z_{\text{upper}}) \rangle$ represents the total charge above, A is the cross-section area of the slab. According to the total charge Q and the area A , the charge density between two plates can be calculated, as shown in Fig. 6B. The value of $\varepsilon(E_{\text{ext}})$ denotes the whole system dielectric constant under an external electric field, E_{ext} , which is obtained from the Equation 5.

The induced field without external field is shown in Fig. 6C. Although the local E -field oscillated, the up and down amplitudes canceled each other to zero, almost resulting in the zero field as a whole.

The influence of different slab thicknesses, $2d$, was also tested. A fictitious plate may divide a neutral water molecule into two parts, namely, the upper one and the bottom one. The resultant two fragments above and below the plate should be negatively or positively charged, respectively. Thus, the induced electric field was generated between two adjacent plates. As depicted in Fig. 6C, the amplitude of fluctuations decreased when we choose the thicker slab.

The fluctuation extent of the induced electric field was rationalized by the charge density on the plate. Taking a snapshot at 0.5 ns, for example, the charge density located at the middle of the z direction (10.9 Å) was analyzed. As shown in Fig. 6B, the calculated charge density corresponding to the usage of slab of 0.4 Å thickness is slightly smaller than the other two, $d = 0.1$ Å and $d = 0.5$ Å, respectively.

In a water molecule, the distance between O atom and the middle point of two H atoms is 0.612 Å. Such a distance is happened to fall within the range of $2d = 0.6 \sim 0.8$ Å. When the thickness, d , approaches to 0.5 Å, i.e., $2d = 1.0$ Å, the possibility of cutting another water molecule into two parts is increased so as to rise up the fluctuation extent of induced electric field.

Applying the same model to the simulation cell with external electric field, the $E(z)$ under different external E -fields, is shown in Fig. 6D. From Fig. 6D, one could conclude that when larger electric field was applied externally, the local electric field varied more significantly. This was consistent with the phenomenon observed from the distribution of dipole orientations in Fig. 2, where the water molecules packed more orderly under the applied E -field (Fig. 3). When the external electric field was added up to $2.175 \text{ V} \cdot \text{nm}^{-1}$ in this work, no evident restructuring transition to the ice-like ordered water was observed. This was in good agreement with the threshold value of electric field, between 5 and $10 \text{ V} \cdot \text{nm}^{-1}$ for the phase

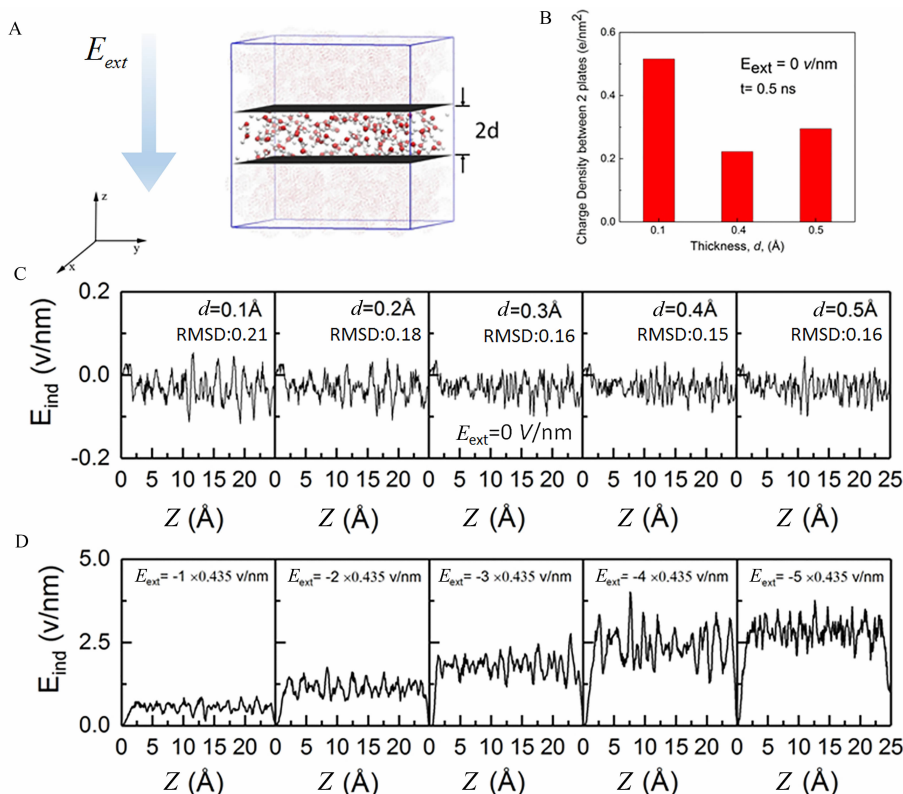


Fig. 6 Comparison of different thicknesses and induced local electric fields under different external electric fields. A. Illustration of the thickness used; B. Charge density on the plate with different thicknesses; C. Induced local electric field of different slab thicknesses when $E_{\text{ext}} = 0 \text{ V} \cdot \text{nm}^{-1}$; D. Induced local electric field of simulations under different external electric fields.

transition of bulk water, as proposed by Yeh^[10].

2.4 The Relationship between the Induced Dipole and the External Field

To better study the influence of the structure changes, interaction between induced-dipole and external field was addressed in detail. Usually Equation 7 is used to calculate the dipole-electric field interaction, \bar{W} .

$$\bar{W} = -\vec{M} \cdot \vec{E}_{\text{ext}} \quad (7)$$

As expected, the dipole-electric field interaction energy, \bar{W} , was zero without the applied electric field, where \vec{M} denoted the total dipole moment of the system, \vec{E}_{ext} is the applied external electric field. It reflected the orderliness of the system to some extent. The interaction between the total dipole moment and external electric field is increased with the increase in the strength of electric field. The interaction energy was increased up to $-1086.03 \text{ kcal} \cdot \text{mol}^{-1}$, when $E_{\text{ext}} = -2.175 \text{ V} \cdot \text{nm}^{-1}$.

More details of the dipole moment per water molecule, dipole-electric field interactions (\bar{W}) are listed in Table 1. The magnitude of induced dipole moment per water molecule, \bar{M}/N , was the averaged value over several frames of the last 1 ns trajectory. E_{total} was composed of the energy of bonded and non-bonded terms as well as external electrostatics energy under the applied electric fields.

3 Conclusions

We have investigated the bulk water in a cubic periodic box under different electric fields. With or without the external electric field, the packing structure varied a little, except for the orientation of dipole moment of individual water molecules. The restructuring transition was not observed when the electric field was lower than the critical value, in agreement with the previous predictions^[10-11].

An exponential decay curve of the relative dielectric constant was shown as a function of the ex-

Tab. 1. Summary of total dipole moment, dipole-electric field interaction and ratio of dielectric constant under different external electric fields

	$E_{\text{ext}}/(\text{V} \cdot \text{nm}^{-1})$					
	0	-0.435	-0.870	-1.305	-1.740	-2.175
$\vec{M}/N(\text{Debye})$	0.29	1.79	2.04	2.13	2.21	2.26
$W/(\text{kcal} \cdot \text{mol}^{-1})$	0	-172.32	-391.65	-619.51	-853.67	-1086.03
$E_{\text{total}}/(\text{kcal} \cdot \text{mol}^{-1})$	-3141.02	-3371.68	-3610.31	-3852.95	-4105.04	-4319.68
$\varepsilon(E_{\text{ext}})/\varepsilon(0)$	1.0	0.283	0.157	0.105	0.081	0.071

ternal electric field when the applied external electric field was about $-0.435 \sim -2.175 \text{ V} \cdot \text{nm}^{-1}$. The amplitude of the local induced electric field increased with the enhancement of the external electric field. The acceleration in convergence rate of G_k was observed, which means that the applied external electric field could speed up the calculation of dielectric constant.

This work gives a general trend and a prediction of relative dielectric constant under high electric fields, which is helpful for understanding the electrostatic polarization and distribution of local induced electric fields. Aimed at the simulations of more complicated systems, such as the biosystems, the field-dependent dielectric constant instead of the explicitly polarizable solvents can be used to speed up the calculation of electrostatic interaction in MD simulations, by representing the local electrochemical environment with local induced field.

Acknowledgement

This work was supported by the National Natural Science Foundation of China (Grant No. 21673111). We are grateful Mr. Tianhao Li from Tsinghua University for his stimulating discussion.

References:

- [1] Nymeyer H, Zhou H X. A method to determine dielectric constants in nonhomogeneous systems: application to biological membranes[J]. *Biophysical Journal*, 2008, 94(4): 1185-1193.
- [2] Archer D G, Wang P M. The dielectric constant of water and debye-hückel limiting law slopes[J]. *Journal of Physical and Chemical Reference Data*, 1990, 19(2): 371-411.
- [3] Wasserman E, Wood B, Brodholt J. Molecular dynamics study of the dielectric constant of water under high pressure and temperature conditions[J]. *Berichte der Bunsengesellschaft für physikalische Chemie*, 1994, 98(7): 906-911.
- [4] Berendsen H J C, Grigera J R, Straatsma T P. The missing term in effective pair potentials[J]. *Journal of Physical Chemistry* 1987, 91(24): 6269-6271.
- [5] Jorgensen W L, Chandrasekhar J, Madura J D, et al. Comparison of simple potential functions for simulating liquid water[J]. *The Journal of chemical physics*, 1983, 79(2): 926-935.
- [6] Saint-Martin H, Hernándezcobos J, Bernaluruchurtu M I, et al. A mobile charge densities in harmonic oscillators (MCDHO) molecular model for numerical simulations: The water-water interaction[J]. *The Journal of Chemical Physics*, 2000, 113(24): 10899-10912.
- [7] Guillot B. A reappraisal of what we have learnt during three decades of computer simulations on water[J]. *Journal of Molecular Liquids*, 2002, 101(1): 219-260.
- [8] Gereben O, Pusztai L. On the accurate calculation of the dielectric constant from molecular dynamics simulations: The case of SPC/E and SWM4-DP water[J]. *Chemical Physics Letters*, 2011, 507(1): 80-83.
- [9] Sprik M. Hydrogen bonding and the static dielectric constant in liquid water[J]. *The Journal of Chemical Physics*, 1991, 95(9): 6762-6769.
- [10] Yeh I C, Berkowitz M L. Dielectric constant of water at high electric fields: Molecular dynamics study[J]. *The Journal of Chemical Physics*, 1999, 110(16): 7935-7942.
- [11] Sutmann G. Structure formation and dynamics of water in strong external electric fields[J]. *Journal of Electroanalytical Chemistry*, 1998, 450(2): 289-302.
- [12] Phillips J C, Braun R, Wang W, et al. Scalable molecular dynamics with NAMD[J]. *Journal of Computational Chemistry*, 2005, 26(16): 1781-1802.
- [13] David V D S, Lindahl E, Hess B, et al. GROMACS: fast, flexible, and free[J]. *Journal of Computational Chemistry*, 2005, 26(16): 1701-1718.
- [14] Case D A, Darden T A, et al. AMBER 9[CP]. University

- of California: San Francisco, 2006.
- [15] Raabe G, Sadus R J. Molecular dynamics simulation of the dielectric constant of water: The effect of bond flexibility[J]. The Journal of Chemical Physics, 2011, 134(23): 234501.
- [16] Soper A K, Silver R N. Hydrogen-hydrogen pair correlation function in liquid water[J]. Physical Review Letters, 1982, 49(7): 471-474.
- [17] Soper A K. The structure of liquid water at room temperature[J]. Chemical physics, 1984, 88(1): 187-197.
- [18] Soper A K, Phillips M G. A new determination of the structure of water at 25 °C[J]. Chemical Physics, 1986, 107 (1): 47-60.
- [19] De Leeuw S W, Perram J W, Smith E R. Simulation of electrostatic systems in periodic boundary conditions. III. Further theory and applications[C]//Proceedings of the Royal Society of London A: Mathematical, Physical and Engineering Sciences, The Royal Society, 1983, 388(1794): 177-193.
- [20] Allen M P, Tildesley D J. Computer simulation of liquids [M]. Oxford University Press, 1989: 95-98.
- [21] Lamoureux G, MacKerell Jr A D, Roux B. A simple polarizable model of water based on classical drude oscillators[J]. The Journal of Chemical Physics, 2003, 119(10): 5185-5197.
- [22] Lamoureux G, Harder E, Vorobyov I V, et al. A polarizable model of water for molecular dynamics simulations of biomolecules[J]. Chemical Physics Letters, 2006, 418 (1/3): 245-249.
- [23] Braun D, Boresch S, Steinhauser O. Transport and dielectric properties of water and the influence of coarse-graining: Comparing BMW, SPC/E, and TIP3P models[J]. The Journal of Chemical Physics, 2014, 140(6): 064107.
- [24] Evans W A B, Powles J G. The computer simulation of the dielectric properties of polar liquids. The dielectric constant and relaxation of liquid hydrogen chloride [J]. Molecular Physics, 1982, 45(3): 695-707.
- [25] Humphrey W, Dalke A, Schulten K. VMD-Visual molecular dynamics[J]. Journal of Molecular Graphics, 1996, 14 (1): 33-38.
- [26] Wilson M A, Pohorille A, Pratt L R. Molecular dynamics of the water liquid-vapor interface[J]. Journal of Physical Chemistry, 1987, 91(19): 4873-4878.

外部电场下水分子间静电相互作用的 分子动力学研究

朱 强, 阚子规, 马 晶*

(南京大学化学化工学院, 介观化学教育部重点实验室, 江苏 南京 210093)

摘要: 本文利用分子动力学模拟探讨了不同外电场下, 液态水的分子间作用及分子排布的变化. 在不同外电场下, $\text{O}\cdots\text{O}$ 原子间的径向分布函数差别很小, 但是单个水分子的偶极矩的取向变化却很大. 当外电场为 0 时, 单个水分子偶极取向的范围很宽 (30 ~ 150 度). 与此同时, 本文给出了局域诱导电场随着位置的变化关系图. 当外加电场增强时, 局域的诱导电场强度也随之增加. 由于电场下偶极矩有序性的增加, 局域诱导的静电相互作用能显著增加. 计算结果表明, 相对介电常数随着电场强度的增加而呈现指数衰减的变化形式. 这一变化趋势可以用来理解不同电化学环境下, 静电相互作用和局域诱导电场的变化.

关键词: 径向分布函数; 介电常数; 平均场模型; 诱导电场; 偶极矩